Propeller Open Water Characteristics in Waves

Propeller Open Water Characteristics in Waves

Mohsen Irannezhad[1,*], Martin Kjellberg[2], Rickard E. Bensow[1], and Arash Eslamdoost[1]

[1]Chalmers University of Technology, 412 96, Gothenburg, Sweden
[2]SSPA Sweden AB, 412 58, Gothenburg, Sweden
[*]Corresponding author, E-mail: mohsen.irannezhad@chalmers.se

INTRODUCTION

The propulsion factors for ships when operating in waves deviate from those in calm water (Gerritsma et al. (1961), Moor and Murdey (1970) and Nakamura and Naito (1975)). Propeller-hull interaction effects are also different in waves compared to calm water. In order to map the differences in an ongoing research, the performance of a tanker ship in calm water and in regular head waves is being studied through the following steps:

1. bare hull performance in terms of resistance, motions and nominal wake in a range of operational conditions,
2. isolated effects of waves on performance degradation of the open water propeller,
3. propeller-hull interaction effects in self-propulsion.

The main objective of this paper is to study the propeller open water (POW) performance in waves and compare it with calm water condition, representing step 2. To this end, a series of POW model tests are carried out in a towing tank for a range of regular head wave conditions. The propeller submergence is chosen to avoid propeller ventilation, while still being affected by the encountered waves. The tests are carried out for a series of advance ratios and wave steepnesses. The desired advance ratios are obtained by keeping the carriage speed constant and adjusting the propeller rotational speed. Numerical computations are also carried out for the same conditions using a Reynolds-Averaged Navier-Stokes (RANS) solver and validated against the model tests. The propeller characteristics including its thrust, torque and efficiency are studied. This paper presents the progress of the research and may be subjected to significant revisions.

APPROACH

The propeller open water model tests are carried out at SSPA towing tank with the length of $260m$. The propeller geometry model is $KP458$, originally designed by MOERI for the second variant of the MOERI tanker (KVLCC2), with the scale factor of 45.714 (propeller diameter $D \approx 0.21m$) and operating in fresh water with the density of $\rho = 998.83kg/m^3$. The propeller geometry and the POW tests setup are shown in Figure 1. A wide range of advance ratios J are tested in calm water while only advance ratios 0.35, 0.45, 0.55 and 0.60 are considered for the tests in waves. All the tests in waves as well as the majority of the tests in calm water are carried out keeping the carriage speed constant ($U = 1.177m/s$ representing the KVLCC2 design Froude number $Fr = 0.142$ at the current scale $L = 7m$) and varying the propeller rotational speed n in order to achieve the desired advance ratios $J = U/nD$. Although more than four J tested in each POW run (from the start to the end of the towing tank) in calm water, only two J are tested in waves during each carriage run. The sampling frequency of all measurement equipment is $100Hz$.

Before carrying out the POW tests in waves at the constant carriage speed of $U_{cte} = 1.177m/s$, wave calibration tests were carried out in order to examine the quality of the generated waves in the towing tank with regards to the wave maker performance and limitations. The expected wave condition (non-dimensional length λ/L, height H, steepness H/λ and encounter period $T_E = 2\pi/(\omega + \frac{\omega^2 U}{g})$ (in which ω is wave frequency and g is the gravitational acceleration) are shown in Table 1. During the POW tests in waves, it was found that the waves deviated from being a regular wave closer to the wave maker, hence some of the tests were repeated in the swapped order of J in the same wave condition. All the tests results are shown in Figure 8b but there is no uncertainty analysis provided for the repeated tests.

For the RANS simulations, a commercial CFD solver, Simcenter STAR-CCM+ (version 2020.3.1) is used. An arbitrary dummy shaft is added to the geometry in order to represent the employed shaft at the POW tests, see

$\lambda/L(-)$	$H(m)$	$H/\lambda(\%)$	$T_E(s)$
0.570	0.042	1.052	1.086
0.570	0.070	1.754	1.086
0.570	0.120	3.007	1.086
1.078	0.133	1.762	1.637

Table 1: Expected wave conditions from the wave calibration tests.

Figure 1: Propeller geometry and POW test setup.

Figures 1 and 2. The shaft length is considered to be long enough to have negligible effects from the flow vortices generated at the shafts end on the upstream flow and hence, propeller performance.

The computational domain is discretized employing a Sliding Mesh Topology which consists a rotating inner region (for the propeller blades and its hub) and a stationary outer region (for the background mesh and propeller boss and shaft), see Figure 2a. An interface at the intersection of the regions are defined through which the information is exchanged between the outer and inner regions. The distance of the propeller center to the computational domain boundaries in the front and back side of the propeller in X direction is approximately $21.3D$, from the sides in Y direction is about $3.6D$ and from top and bottom in Z are 15.7 and $19.8D$, respectively. The propeller submergence, i.e., vertical distance from propeller center to the undisturbed free surface, is $1.5D$.

Unstructured grids including the trimmed hexahedral meshes with local refinements near the free surface and near the propeller in the outer region and the polyhedral meshes near propeller blade and hub in the inner region are generated. Moreover, prism layer meshes along the propeller surface as well as both sides of the interface are generated using STAR-CCM+ automatic mesh generator, see Figure 2. The simulations are wall-resolved, therefore, it was aimed to have $y^+ < 1$ approximately all over the geometry. The free surface refinements resulted in approximately 7, 12, 20 and 22 cells per wave height in Z for the wave heights shown in Table 1. The cell dimensions in X and Y at the free surface are four times larger than in Z direction. For the simulations, the $5th$ order Stokes wave is applied at the boundaries of the computational domain which are found to be a better resemblance of the natural waves than airy waves. A wave forcing function in STAR-CCM+ in the vicinity of the front and back boundaries in X direction are applied to a distance of $14.8D$ in order to force the solution of the discretized Navier-Stokes equations towards the theoretical $5th$ order Stokes wave solution, hence minimizing the wave reflections from the boundaries. More detailed simulation configurations for the wave propagation simulations are provided in Irannezhad et al. (2021). Although computationally inefficient, the same mesh is used both for simulations in calm water and in waves in order to diminish the possible sources of discrepancy. The total number of cells in the outer and inner regions are $4.0M$ and $10.6M$, respectively.

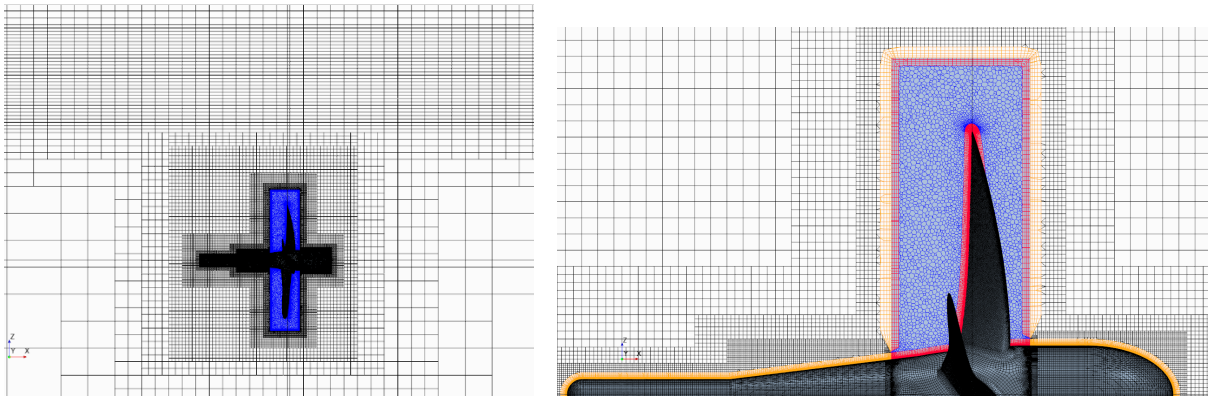

(a) Inner and outer regions.

(b) Zoomed half geometry mesh.

Figure 2: Overview of the computational grid near the propeller. Black lines represent the mesh in the outer region. Blue lines represent the mesh in inner region. Red and Orange colors represent the prism layers in inner and outer regions, respectively.

The Volume of Fluid (VOF) model is used to capture the free surface. The High Resolution Interface Capturing (HRIC) scheme by Muzaferija and Peric' (1999) is used in VOF simulations to maintain a sharp interface between the incompressible fluid phases. The propeller rotational speed n is applied to the inner region. Moreover, a tangential velocity boundary condition at the propeller boss and shaft are applied in order to have wall relative rotation with the same local rotational rate n as in inner region. An implicit unsteady solver is used with a second order temporal discretizational scheme. The time step $dt = 1/(360n)$ is chosen in order to have 1° of propeller rotation per time step. Furthermore, 20 inner iterations are considered to ensure the convergence of the simulation in each time step.

k-ω SST turbulence model is employed for the simulations. Due to the size of the propeller diameter ($21cm$) and its operating conditions, the Reynolds number at the higher advance ratios approached the laminar flow range, resulting in dominance of laminar flow on the blades. For the lower J values, the flow near wall is a combination of laminar, transitional and turbulent flow. Therefore, a transition model, Gamma Re-Theta is also used in the computations to model the transition from laminar to turbulent flow on the blades, see Figure 3. The flow regime has significant effect on the propeller performance. In order to investigate the effects of flow regime on the propeller, a set of POW tests in calm water are carried out in which the propeller rotational speed is considered to be constant (n_{cte}) and instead the carriage speed is varied in order to derive the desired advance ratios. The results are shown in Figure 8b. It is seen that at the higher J values, the propeller efficiency is higher for the model tests with n_{cte} (lower Reynolds number) compared to U_{cte}. This means that the K_T/K_Q for n_{cte} is higher, hence lower torque and therefore, laminar flow dominance on the blades.

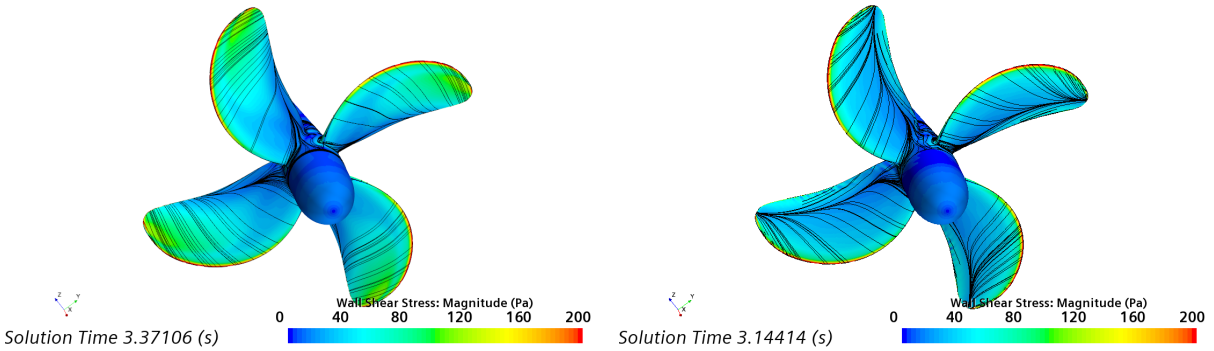

(a) Without transition model - fully turbulent.

(b) With transition Model.

Figure 3: The effect of transition model on the wall shear stress and limiting streamlines on the flow over the suction side of the blades in calm water simulations.

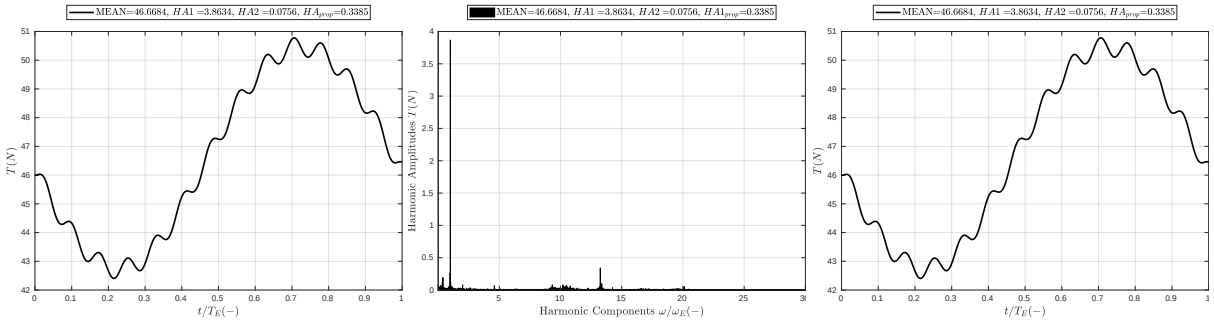

(a) FFT window of the time series.

(b) FFT results.

(c) Reconstructed time series.

Figure 4: Example of time series post-processing method.

Generating perfectly regular waves in experiments in the towing tank is impossible and there are always deviations from the theoretical wave. The waves are playing a significant role on the propeller performance. Therefore, the propeller performance would not show a regular and repetitive behavior. One example of time series from the experiments is shown in Figure 4a. The Fast Fourier Transform (FFT) is employed in order to find the harmonic amplitudes at the harmonic components ω/ω_E of the signal and shown in Figure 4b. Different cautions are taken into account to minimize the possible spectral leakage in the FFT process. The $0th$ harmonic amplitude ($MEAN$ value) as well as the $1st$ and $2nd$ harmonic amplitudes ($HA1$ and $HA2$) at the wave encounter frequency, i.e., $\omega/\omega_E = 1\&2$, together with the $1st$ harmonic amplitude at the blade passing frequency $2\pi n$ ($HA1_{prop}$) are computed and shown in the legends of the plots in Figure 4. Thereafter, the dominant harmonic amplitudes in both the wave encounter frequency and the blade passing frequency of the propeller are used in order to reconstruct the time series to show it only for one encounter wave period, see Figure 4c.

RESULTS

The results for $J = 0.35$ and 0.55 are shown in Figures 5 and 6, respectively. The results include the reconstructed time series for the wave height at the propeller plane H_{pp}, thrust coefficient $K_T = T/\rho n^2 D^4$, torque coefficient

$10K_Q = 10Q/\rho n^2 D^5$ and propeller open water efficiency $\eta_O = JK_T/2\pi K_Q$. The wave height in the model tests is measured at a wave probe located $4.68m$ in front of the propeller plane and then synchronized based on the carriage speed and wave group velocity in order to represent the wave at the propeller plane. The generated numerical wave is very similar to the theoretical wave, hence the theoretical wave characteristics are used in CFD results. For clearer representation of result, only one condition is shown for the CFD data in waves. In the plot legends, the incident wave characteristics, advance ratio, and important harmonic amplitudes for the respective condition are provided.

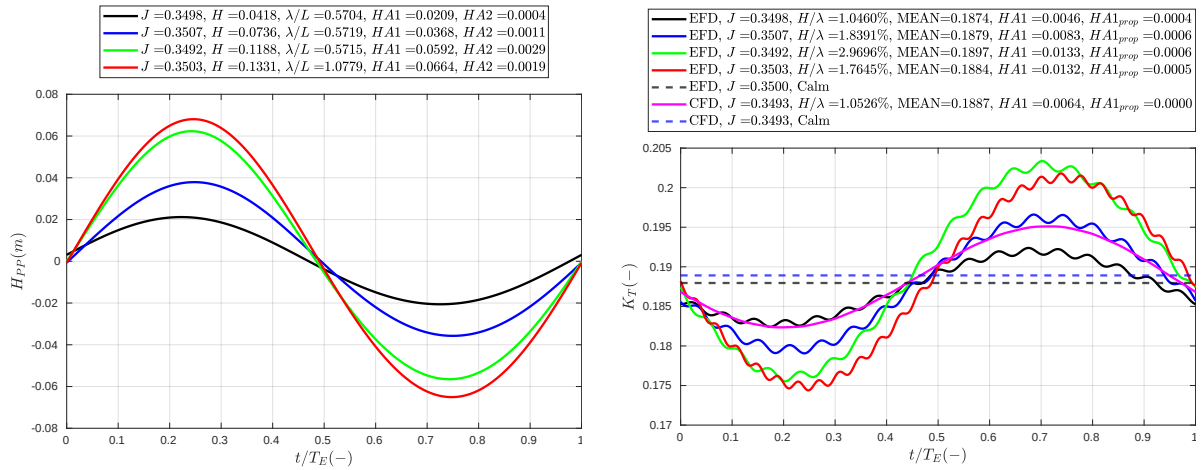

(a) Wave height at propeller plane.

(b) Thrust coefficient.

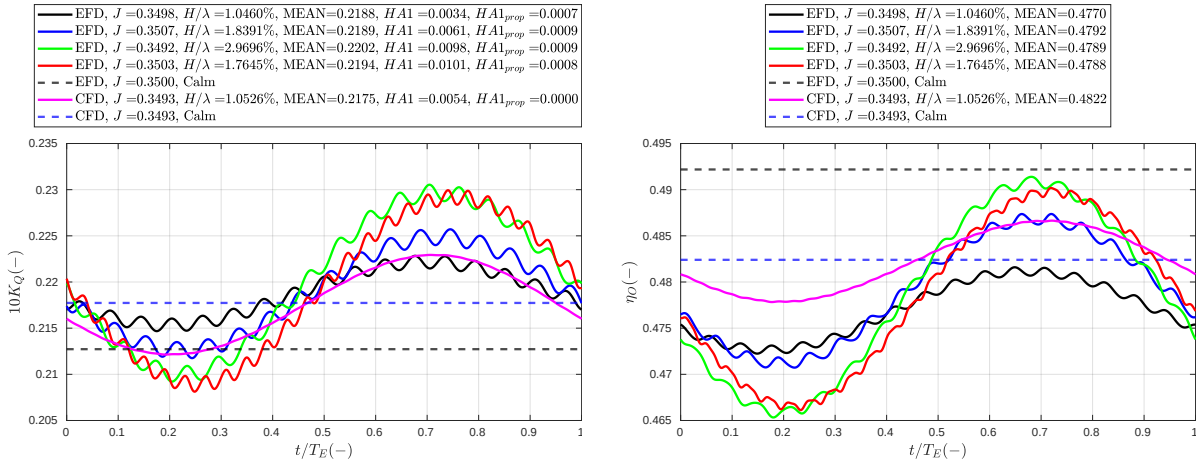

(c) Torque coefficient.

(d) Propeller efficiency.

Figure 5: Reconstructed time series for advance ratio $J = 0.35$.

Propeller loading varies in waves. K_T, K_Q and η_O are increasing at the wave trough and decreasing at the wave crest. This is due to the non-uniformity in the propeller inflow as a function of the orbital wave velocities. The orbital velocities of the wave change the instantaneous advance ratio J for the propeller. The amplitude of oscillations in each respective propulsion factor is larger for the higher J values, comparing Figures 5 and 6. Moreover, the amplitude of oscillation in each J increases for the higher waves with the same wave length. It is interesting that the amplitude of oscillations is not directly connected to the wave steepness H/λ, instead the wave height H is the dominant parameter per se. This can be observed by comparing the red and blue lines with almost the same wave steepness but different wave lengths.

Comparing the EFD and CFD results for the similar corresponding wave conditions shows similar propeller loading oscillations during T_E. In Figure 7, the iso-surface defined with Q-criterion $= 10000/s^2$ and colored by normalized helicity is shown for the CFD simulation of $J = 0.5490$ - $\lambda/L = 0.5700$ - $H/\lambda = 3.0075\%$ at two instances of wave crest and wave trough at the propeller plane. Higher propeller loading when the wave trough is at the propeller plane can be observed through stronger vortical structures in the flow especially at the tip of the blade.

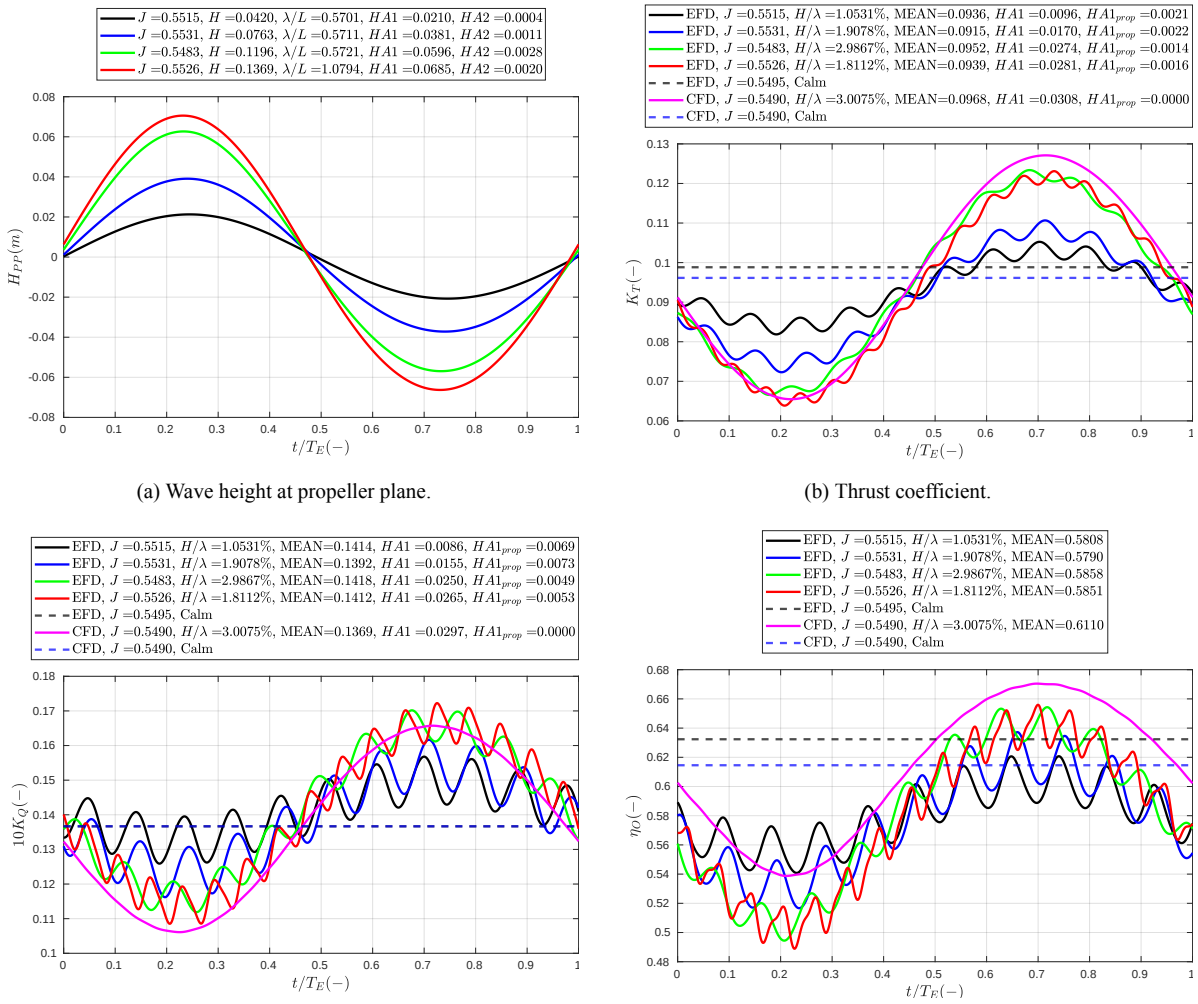

(a) Wave height at propeller plane.

(b) Thrust coefficient.

(c) Torque coefficient.

(d) Propeller efficiency.

Figure 6: Reconstructed time series for advance ratio $J = 0.55$.

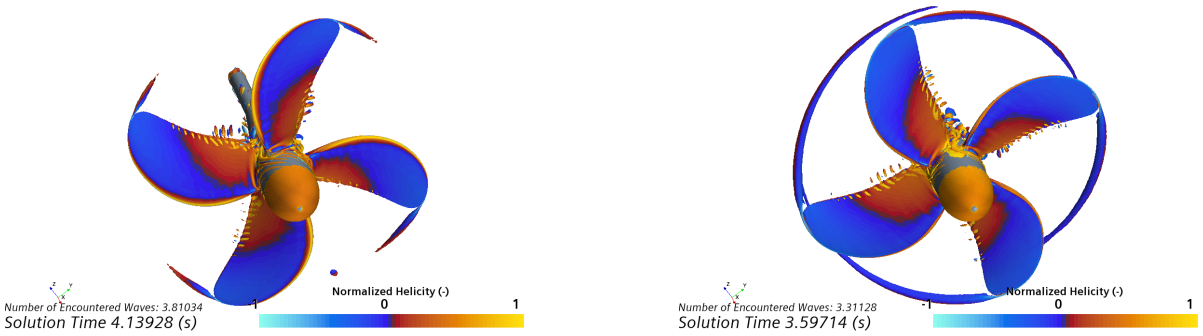

(a) Wave crest.

(b) Wave Trough.

Figure 7: Q-Criterion iso-surface at two time instances of the incident wave in a CFD simulation.

The main difference between CFD and EFD is the oscillations at the propeller blade passing frequency in EFD which is missing in the CFD time series. It is believed that the shaft line vibrations caused by asymmetry of the flow into the propeller (e.g., slight shaft inclination) in the POW tests is the main reason for such discrepancies. In order to investigate more on this matter, the propeller torque on a single blade in a CFD simulation ($J = 0.5490$ - $\lambda/L = 0.5700$ - $H/\lambda = 3.0075\%$) is monitored during $2T_E$ and multiplied by 4 (as the number of propeller blades) and compared with the full geometry Q in Figure 8a. It is interesting that the one blade torque exhibit oscillations at the blade passing frequency (due to varying induced velocity of the waves at different blade positions) but such

oscillations in the full propeller torque is smoothed out. It is believed that the loading distribution on the blades is cancelled out when the full geometry is taken into account. The comparison of CFD and EFD results also reveals that for the similar corresponding wave conditions, K_T is over-predicted at the wave trough in CFD in comparison to EFD in both J. On the other hand, K_Q is under-predicted at the wave crest in CFD. Consequently, η_O is over-predicted over the whole T_E.

Finally, the propeller open water curves are shown in calm water and in waves in Figure 8b. It is seen that the efficiency in calm water and in waves are the same in the CFD simulations. However, the efficiency in waves is significantly reduced in comparison to the calm water efficiency in the EFD results. This drop of efficiency increases in the higher J values. On the other hand, laminar flow dominance is previously seen in calm water at higher J values. Therefore, it can be concluded that the laminar flow regime is decreased in waves in the EFD data which resulted in the increased propeller torque and hence, lower efficiency. However, this is not true in CFD and consequently, there is a difference in the flow regime between CFD and EFD. Although there was a waiting time between POW model tests, the perturbations from the wave maker and the previously generated waves at the towing tank may have triggered an earlier transition to turbulent flow in the towing tank tests.

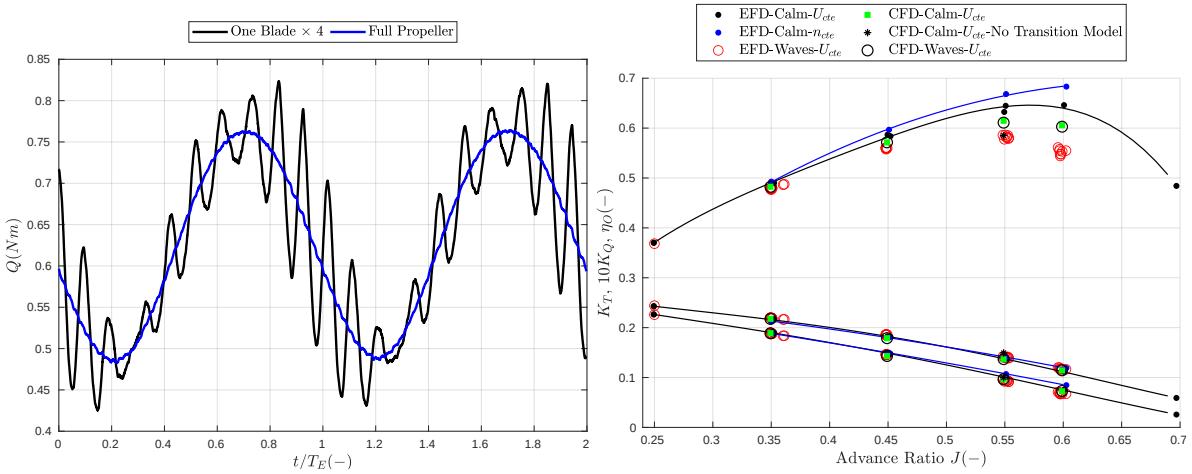

(a) CFD torque comparison.

(b) Propeller open water curves.

Figure 8: Comparison of CFD torque for one blade multiplied by 4 and the full propeller geometry torque and propeller open water curves in calm water and regular head waves.

CONCLUDING REMARKS and FUTURE WORK

It is seen that the propeller loading varies in waves; increased at wave trough and decreased at wave crest. Moreover, there are oscillations at the blade passing frequency of the propeller in the EFD results, however, such oscillations are missing in the CFD results. It is planned to perform a simulation having slightly inclined propeller to reproduce the propeller blade passing frequency oscillations seen in the EFD results.

It seems that the laminar flow dominance in model scale is a challenge in simulation of propeller flow, as the flow regime on the blades in waves is different than in calm water. One hypothesis is that the waves working as a perturbation which may trigger an earlier flow transition on the blades. A sensitivity analysis of the transition model to the upstream turbulence intensity is planned.

The effects of domain size especially in Y direction as well as the local grid refinements especially behind the propeller (for a more accurate prediction of propeller wake and its effects on propulsion factors) as well as in front of propeller (for a more accurate wave orbital velocities capturing into the propeller) will be studied in future. Moreover, the propeller performance characteristics will be studied at another submergence in order to investigate the effect of submergence on propulsion factors.

REFERENCES

Gerritsma, J., van den Bosch, J., Beukelman, W., 1961. Propulsion in regular and irregular waves. Int. Shipbuild. Prog. 8 (82), 235–247. http://dx.doi.org/10.3233/ISP-1961-88201.

Moor, D.I., Murdey, D.C., 1970. Motions and propulsion of single screw models in head seas, Part II. Trans. R. Inst. Nav. Archit. 112 (2).

Nakamura, S., Naito, S., 1975. Propulsive performance of a container ship in waves. J. Soc. Nav. Archit. Japan 15 (158).

Irannezhad, M., Bensow, R. E., Kjellberg M., and Eslamdoost A. (2021). Towards uncertainty analysis of CFD simulation of ship responses in regular head waves. In: Proceedings of the 23rd Numerical Towing Tank Symposium.